# Effect of Milling Time, Doping Concentration and Temperature on the Structural, Microstructural and Optical Properties of Cu Doped ZnO Nanoceramics

**Dr. Bikram Keshari Das**
Kalinga Institute of Social Sciences(KISS) Deemed to be University, Bhubaneswar
**Dr. Tanushree Das**
Kalinga Institute of Social Sciences(KISS) Deemed to be University,bhubaneswar
**Dr. Kajal Parashar**
KIIT University
**SKS Parashar** ( sksparashar@yahoo.com )
KIIT University
**Dr.Rajeev Kumar**
Indian Institute of Science,Banglore
**Dr. Anupama A. V.**
Indian Institute of Science,Banglore
**Dr.Balaram Sahoo**
Indian Institute of Science,Banglore

**Research Article**

**Keywords:** High energy ball milling, XRD, Rietveld, FESEM, TEM, DRS

**Posted Date:** April 1st, 2020

**DOI:** https://doi.org/10.21203/rs.3.rs-20283/v1

# Abstract

In this work, high energy ball milling (HEBM) technique has been employed to successfully synthesize a series of Cu-doped ZnO nanoceramics (Zn 1-x Cu x O) with Cu concentration x = 0, 0.01, 0.02, 0.03 and 0.04. The synthesized nanoceramic was analysed by XRD, FESEM, TEM, Uv-Vis-DRS. The structural, microstructural and optical properties of the synthesized sample with different duration of milling, doping concentration and temperature has been investigated. X-ray diffraction result indicates that the samples are wurtzite structure with single phase. A decrease in peak intensity was observed with increase in milling time. 10h milled Cu doped ZnO sample shows single phase. After calcination at 900 ºC in x = 0.04 few peaks related to CuO was observed indicating the solubility limit of Cu in ZnO is 3 atomic%. With increase in milling time crystallite decreases where as strain increases however after calcination crystallite increases where as strain decreases. After calcination peak intensity increases. The specific surface area of ZnO increases after Cu doping but decreases after calcination. Bond length decreases after calcination but lattice distortion increases. FESEM micrograph shows particle growth after calcination. The average particle size decreases with increase in Cu concentration(30 nm to 20 nm) whereas increases after calcination and sintering (488 nm-2706 nm).The band gap decreases with increasing in milling time also with increase in Cu concentration and after calcination. Cu doping in ZnO shows red shift indicating Cu doped ZnO samples are suitable for optoelectronic device applications.


# 1. Introduction

ZnO has outstanding properties with a direct band gap of 3.37eV, large exciton binding energy of 60 meV, transparent, nontoxic, cheap, high physical and chemical stability, semiconducting behaviour with unparallel piezoelectric, thermal, optolectronic and transport properties. Because of these peculiar properties, ZnO is the material of preference for a broad range of applications like optoelectronics, transparent electronics, spintronic and sensor devices [1,2],UV screening applications [3]. Properties of zinc oxide can be modified by incorporation of transition metals for different applications. Different dopants like Cu, Cr, Co, Mn, Ni etc. are doped into the ZnO which brings major change in the physical and chemical properties [4]. Doping by other elements such as Al, Ga, Ti, Li, Eu, Ce, Y, La, Er, Au, and Pb into ZnO lattice have also reported in the literature. Despite the potential doping of these elements, Cu is selected as dopant for the present investigations as it shows many interesting applications as fluorescent sensor, acetone and ethanol gas sensor, $H_2S$ gas sensing, CO gas sensor, resistive random access memory, and diluted magnetic semiconductors [5]. Different synthesis methods like auto-combustion [6], ball milling [7], co precipitation [8], sol gel [9], hydrothermal [10] etc. are used for the preparation of transition metal doped ZnO nanoparticles. High energy ball milling was found to be a very efficient method for production of nanoparticles in a large scale with grain size ~100 nm [11]. The chemical reaction takes place between the constituent powder phases during ball milling which brings structural and morphological changes in the particles as well as the electrical and optical properties of materials [12].

The imperfect crystallinity of crystal develops XRD peak broadening. The properties like (a) crystallite size and (b) lattice strain can be extracted from the analysis of peak width. Because of polycrystalline aggregate crystallite size and particle size is not same [13]. Different analysis techniques like BET, SEM and TEM are used for the particle size measurement. Lattice strain arises from crystal imperfections such as lattice dislocation, grain boundary triple junction, sintering etc. [14]. High energy ball milling also brings about a huge strain in the samples [15]. Crystallite size and lattice strain can be analysed by X-ray profile analysis [16]. The characterization of nanocrystalline materials can be done with regard to (i) grain size and (ii) lattice defects [14, 17]. The sintering temperature, doping of metal plays an important role for changing properties like optical, electrical etc. [18, 19]. The study on band gap reduction effect of ZnO based oxides have thus paying attention of intense research [20].

In the present work we have investigated extensively the structural, morphological and band gap tuning of Cu doped ZnO nanoceramics synthesised by high energy ball milling.

# 2. Materials And Method

Nanocrystalline Zn1-xCuxO (x = 0, 0.01, 0.02, 0.03 and 0.04) was synthesized by High Energy Ball Milling method (HEBM, PM400Retsch, Germany). Stochiometric amount of ZnO and CuO were taken according to their atomic ratio in tungsten carbide vials with tungsten carbide balls in ball to powder ratio 3:1 and were milled for 10h with an altering stop of 30 min after each 1hr of milling to prevent wear at a speed of 300 rpm. The synthesized powders were calcinated at 900 ºC at a heating rate of 2 ºC/min. The structural parameters of 10h milled calcined powder was carried out by using XRD (D8 Advance, Bruker) at room temperature. The morphologies of the ball milled powder, the pellet sample after calcinations at 900 ºC for 2h and also for the 900 ºC sintered pellet was investigated by Field Emission Scanning Electron Microscopy (FESEM, Carl Zeiss NTS Ltd, UK). The Transmission Electron Microscopy (TEM) of the synthesized sample was carried out by the JEOL 2010 TEM with 200 kV acceleration voltages. The UV-Vis absorption spectrum of the samples was recorded via the use of Lambda 750 UV/Vis/NIR Perkin Elmer spectrophotometer. The Rietveld refinement of the XRD patterns was performed by using the “FullProf” program.

# 3. Results And Discussion

### 3.1 Structural analysis-XRD

#### 3.1.1 Effect of milling time

Figure 1 shows the XRD pattern of pure ZnO, pure CuO and 10h ball milled ZnO samples. From the Figure it was clearly observed that the peak intensity high at 0h which is decreased after 10h milling. The intensity of Pure ZnO is higher than that of pure CuO.

The room temperature XRD pattern of $Zn_{1-x}Cu_xO$ (x = 0, 0.01, 0.02, 0.03 and 0.04) nanoceramics at different milling times (0, 2, 4, 6, 8, 10h) were shown in Figure 2 (a, c, e, g and i) and their enlarged view

are shown in Figure 2 (b, d, f, h and j) respectively. The highest intensity peak is along (101) plane and the shifting of this plane for different duration of milling was shown in Figure 3 (a-e).The XRD pattern of 0h (unmilled) sample shows distinct peaks belonging to the starting oxides of CuO and ZnO. The strongest peak at 2θ≈38.74º correspond to the principal peak of CuO (marked as Δ, Figure 2(d, f, h and j)) and peak belonging to ZnO phase (marked as *, Figure 2(c, e, g and i)). The formation of $Zn_{1-x}Cu_xO$ (x = 0-0.04) was observed with 4h of milling itself and further increase in milling time for 10h, the crystallite size reduces to 20nm. The XRD pattern of 10h milled $Zn_{1-x}Cu_xO$ samples clearly shows the crystalline behaviour. The peak shows that crystal structure of $Zn_{1-x}Cu_xO$ nano powders are similar to JCPDS data card No. 36-1451 [21-26]. A decrease in peak intensity and peak broadening observed due to ball milling which indicates the reduction in size of the sample. This expansion of peak confirmed the decrease in size and the improvement of strain in the prepared samples.It is clear from the XRD pattern of 10h milled sample that there is no secondary peak related to CuO or Cu related secondary and impurity phase which confirms the purity as well as formation of single phase of the sample[26-28]

The peak shifting for different duration of milling was observed from (Figure 3) shows the shifting towards the lower 2θ angle.This may be due to various kinds of strain arises in the synthesized samples due to milling and also due to introduction of Cu into ZnO lattice.

### 3.1.2 The effect of milling time on crystallite size (D) and strain (ε)

The variation of crystallite size and strain for different duration of milling time was shown in Figure 4(a-e). The Williamson-Hall method was used to find out the average crystallite size and strain.

From the Figure 4, it was found that with increasing milling time the crystallite size reduces where as the strain enhances i.e. a inverse relationship exist between crystallite size and lattice strain with different duration of milling. The considerable increment in the lattice strain may be due to decrease of size of the powders during milling which led to reduction in crystallite size and increase in lattice strain [29,30]. The crystallite size of the samples ranges from ~101 nm to ~11nm where as the strain in the range of $0.16 \times 10^{-3}$ to $5.02 \times 10^{-3}$ for ZnO and CuO sample. After Copper doping the crystallite size of ZnO reduces where as strain decreases.

### 3.1.3 Effect of calcination temperature

Figure 5(a) shows the XRD pattern of the 10h milled $Zn_{1-x}Cu_xO$ samples with varying Cu concentration. The XRD pattern of 10h milled sample with calcination at 900ºC for 2h was shown in Figure 5(b). The Rietveld refinement of the XRD patterns for these ball milled samples (Figure 6(a-e)) are in good agreement with experimental results. No additional peak related to CuO or any other impurity was found in the X-Ray Diffraction patterns of 10h milled samples upto x = 0.04

The Rietveld refinement XRD of 10h ball milled and calcination at 900ºC was shown in Figure 7(a-e). The X-Ray Diffraction pattern of the 10h milled calcined samples also shows that the samples with Cu concentration up to 3 atomic% (x = 0.03) maintains their structure intact. Figure 5(b) for x = 0.04 few

peaks at 2θ = 35.61° and 38.74° (marked by the symbol Δ) related to low intense peak of CuO were observed. Figure 7(e) agreed with the experimental result. It shows that after 10h of milling, the Cu atoms were diffused into the ZnO and substituted Zn. But after calcination at 900 ºC, sample up to x = 0.03 substituted $Cu^{2+}$ ion retain the $Zn^{2+}$ ion positions in the ZnO, giving single phase $Zn_{1-x}Cu_xO$ material, but above x = 0.03, CuO precipitates, generating CuO peaks in the XRD pattern. This is because after calcination Cu ion diffused in ZnO crystal get separated from ZnO and produce a secondary phase. Similar observation was also reported by Y. Liu et al.[31].

For each sample the FWHM of the XRD peak decrease and the intensity increase as compared to uncalcined sample indicating the decrease in the strain during calcination and the crystallite size have grown larger.

### 3.1.4 Effect of calcination temperature on structural parameters

The structural parameters of 10h milled $Zn_{1-x}Cu_xO$ samples obtained from the Rietveld refinement of the X-ray diffraction pattern using fullprof software [32] was shown in Figure 8(a-f), where as Figure 9(a-f) shows the structural parameter of calcined (900ºC) samples. The change in lattice parameter '*a*' and '*c*' with different Copper concentration were given in Figure 8(a). The lattice constant of ZnO was found to be increased with Cu doping and it was changing regularly up to x = 0.02. The observed variation in lattice parameter related to the variation in ionic radii of $Zn^{2+}$ (0.74Å) and $Cu^{2+}$ (0.73Å) ion [33,34]. The lattice parameter of the calcined sample (Figure 9(a)) shows that it reduces with Cu doping and it enhances linearly with Cu concentration. This also proved indirectly that the $Cu^{2+}$ was substituted into ZnO lattice [35].The c/a ratio shows the hexagonal structure of ZnO is not effected by Cu doping as well as with changing concentration. The volume of the unit cell was calculated by using the equation [36].

$$V = 0.866 \times a^2 \times c \qquad (1)$$

The volume increases slowly with Cu doping (Figure 8(b)), whereas after calcination, the volume decreases (Figure 9(b)). The constant (c/a) ratio shows the hexagonal structure of pure ZnO remain undisturbed after Cu doping or calcination [27].

The crystallite size of ZnO reduces with Cu doping (Figure 8(c)) and also with increase in Cu concentration up to (x = 0.03) but for x = 0.04 it slightly increases, whereas the strain increases linearly. The crystallite size of Cu doped ZnO increases significantly after calcination where as the lattice strain decreases with increase in crystallite size (Figure 9(c)) in comparison to uncalcined sample because of lattice reduction and defect concentration [37]. It is well known fact that the effect of temperature plays a important role in the crystallite size of ZnO nano phase [27].

The variation of specific surface area and u-parameter with Cu concentration for uncalcined sample was shown in Figure 8(d) and for calcined sample in Figure 9(d).

The specific surface area (S) is calculated by using the formula [38]

$$S = \frac{6 \text{ X } 10^3}{Dp.\rho} \quad (2)$$

The Oxygen positional parameter (u) is calculated by using the relation [39]

$$u = \frac{1}{3}\left(\frac{a^2}{c^2}\right) + \frac{1}{4} \quad (3)$$

The specific surface area of ZnO increases after Cu doping for all composition except x = 0.03, where it decreases. Which may be due to increase in particle size as observed from FESEM (Figure 12). However a dramatic decrease in specific surface area was observed after calcination and hence increases the crystallite size. This value of specific surface area of uncalcined sample indicates the higher reactivity of sample [39]. The oxygen position parameter (u) explains the relative dislocation between Zn & O sub lattice along the c-axis. There is a strong relationship lies between the c/a ratio and u parameter. The c/a ratio decreases with distortion of tetrahedral angle. Here an increment in u value was observed with Cu doping as well as with calcination.

The bond length (L) is analyzed by using the relation

$$L = \sqrt{\frac{a^2}{3} + \left(\frac{1}{2} - u\right)^2 c^2} \quad (4)$$

where a and c are lattice parameter and u is the oxygen positional parameter [26,40].

The crystal lattice distortion degree is calculated by using the relation [41]

$$R = \frac{2a\left(\frac{2}{3}\right)^{\frac{1}{2}}}{c} \quad (5)$$

The effect of doping on bond length Zn-O (L) and crystal lattice distortion degree (R) was shown in Figure 8(e) and Figure 9(e) respectively.

This variation in bond length is because of the result of replacement of the ions in ZnO. Change in bond length was observed due to Cu doping, which may cause a some structural disorder in the crystal structure. The bond length reduces after calcination where as crystal lattice distortion (R) increases. The dislocation density (δ) was shown in Figure 8(f) and 9(f) for uncalcined sample and calcined sample respectively. The increase in dislocation density was observed in Cu doped ZnO nanoceramics. Because of the presence of $Cu^{2+}$ ion in ZnO lattice the lattice strain arises. The uncalcined sample shows higher value of δ than the calcined sample, showing highest hardness [38].

# 4. Crystal Structure Super Cell Model

The crystal structure super cell model of ZnO and Cu doped ZnO was created using VESTA software.

In order to achieve realistic experimental dopant concentration, we used periodic 3x3x3 supercell of ZnO and Cu doped ZnO sample using DFT theory, which are drawn from XRD result[26]. The structure of ideal ZnO has a hexagonal wurtzite. Figure 10 represents the supercell of the wurtzite ZnO with total 102 atoms out of which 51 number of Zn atoms and 51 numbers of O atoms.

By substitution of one Zinc (Zn) atom by one Copper (Cu) atom, 1% Cu-doped ZnO results (x = 0.01) (Figure 3.10(b)). It contains 50 atoms of Zn, 1 atom of Cu and 51 atoms of O. Similarly replacing two and three Zn atoms by Cu atoms 2% and 3% Cu-doped ZnO (x =0.02 and 0.03) results. In this case the super cell contains 49 and 48 atoms of Zn with 2 and 3 atoms of Cu respectively and 51 atoms of O which is depicted in Figure 11(c and d). As above 3% Cu precipitates, so Cu is not replacing Zn from its crystal lattice and is placed in the interstitial position. Figure 11(e) shows the supercell of 4%Cu doped ZnO, which contains 48 atoms of Zn with 4 atoms of Cu and 51 atoms of O.

# 5. Microstructural Characterization

Microstructural analysis of the ball milled sample has been carried out by FESEM, EDX and TEM.

Figure 12(i-iii) shows the FESEM micrograph of all ball milled (uncalcined and calcined) $Zn_{1-x}Cu_xO$ samples. The surface morphology of ZnO changes with doping and temperature as observed from FESEM micrograph. The majority of the particles have spherical in shape and the normal particle size is in the nanometric regime. The bigger sized aggregation were noticed with increasing Cu concentration (Figure 12(i)). This nano powder calcined at 900ºC and compacted to prepare the pellet. The similar pattern of increasing particle size was also observed in case of unsintered Cu doped pellets (Figure 12(ii)). This can be due to the agglomeration of particle after calcination. It shows that the calcined/sintered particles are polycrystalline in nature. It has been observed that the relative density of all the samples increases after sintering at 900ºC. However, the relative densities of unsintered samples are less (~92%). After sintering the density of all sample increases to (97-99%). The particle size distribution of all samples was shown in Figure 14 and the adj. R-Square is 0.767. From Figure, it was clear that the average particle size of uncalcined powder is in the range of 18 nm to 37nm (Figure 14(i)). Whereas after calcination the particle size increases from 209 nm to 915 nm (Figure 14(ii)). The particle size of uncalcined Cu doped ZnO sample was also calculated by TEM (Figure 13).

Again after sintering the particle size increases and is within 488 nm to 2708 nm (Figure 14(iii)). It was also found that, the average particle size enhances with increase in copper concentration.

The chemical composition of pure ZnO and Cu doped ZnO ($Zn_{1-x}Cu_xO$) with different concentration of Cu was analyzed by energy dispersive X-ray spectroscopy (EDX) and was depicted in Figure 15(a-e).

Here it is carried out to confirm the presence of dopant. The EDX spectra of pure ZnO consists of only Zn and O while Cu doped ZnO contains Zn, O and Cu which proves the successful doping. The Cu peak

height increases with increasing Cu concentration which shows from Figure 15 that Cu is throughly mixed and diffused into ZnO. The presence of any other element has not been observed in the prepared samples, which confirms the samples are in pure form. This corresponds with the result obtained from the XRD analysis.

# 6. Optical Properties

Studies of optical properties have special importance for optoelectronics applications. The optical properties has been studied by using. UV-Vis Diffuse Reflectance Spectroscopy (DRS).

As ZnO is a direct band gap material [39] and the energy band gap ($E_g$) can be calculated by direct transition between conduction band and valence band [42]. It was determined by plotting the square of the Kubelka-Munk function $F(R)^2$ Vs hv and extrapolating the linear part of the curve to $F(R)^2 = 0$.DRS technique can extract the band gap values of powder semiconductor without any ambiguity.

## 6.1 Effect of milling time on optical energy band gap ($E_g$)

The band gap energy ($E_g$) of ZnO and copper doped ZnO was estimated by using Kubelka-Munk method [43–46]. It promotes the transformation of the measure diffuse reflectance and the extraction of $E_g$ value with best accuracy.

In case of a semiconductor material the band gap energy varies with the crystal defect developed within the material due to doping [47]. In order to see the effect of milling time and size effect on band gap energy ($E_g$), the reflectant spectra of 2% Cu doped ZnO (x = 0.02) was studied with different milling time (2,4,8 and 10) and was shown in Figure 16 and their corresponding $E_g$ value was shown in Figure 17.

The effect of particle size was clearly observed in the bad gap. The gradual red shift was attributed to size reduction and increase in strain during the milling process. The estimated band gap energy ($E_g$) for 2h milled sample was found to be 3.11eV which decreases for 4h and 8h (3.02eV and 2.98eV) which may be because of reduction in crystallite size with increase in milling time, but for 10h milled sample it was found to be 3.09 eV(Figure 17). This investigation is in good agreement with some of the recent reports [48-50]. Thus mechanical milling can be considered as an important tool to control the optical properties of ZnO for optoelectronic device application.

## 6.3 Effect of Cu concentration on optical energy band gap

Figure 18 shows the reflectant spectra of 10h milled calcined $Zn_{1-x}Cu_xO$ nanoceramics. The sharp absorption edge at 372 nm in pure ZnO shifts slightly towards longer wavelength edge for the Cu doped samples may be attributed to increase in grain size after calcination.

It was clearly noticed from Figure 19 that the band gap reduces with doping. A number of researcher also reported that there is a reduction in band gap of ZnO band gap by the introduction of doping element [51-

54]. Again there is regular decrease in band gap of ZnO (red shift) with enhancement in Cu concentration up to 3% Cu doping (x = 0.03) and for x = 0.04, it slightly increases which supports XRD result. Diouri et al. also reported the similar type of red shift in energy band gap for transition metal doped II-VI semiconductor [55,56] which is due to the p-d spin exchange interactions. A reduction in the band gap for Cu doped ZnO nanoparticles was also observed by Elilarassi et al. [57,58].

### 6.3 Effect of calcination temperature on optical energy band gap

This decrease in band gap of ZnO is mainly due to the strong p-d mixing of O and Cu. This is supported by the observation of Bylsma et al. [59]. The red shift in band gap of Cu doped ZnO sample synthesized by ball milling technique confirms the uniform distribution of Cu for Zn in the lattice.

# Conclusion

High energy ball milling technique could successfully lead to the synthesis of Zn1-xCuxO nanoceramics.The pure and doped ZnO samples prepared by high energy ball milling are nanocrystalline with single phase hexagonal wurtzite structure. The crystallite size of both ZnO and Cu doped ZnO sample decreases where as strain increases with increase in milling time. After calcination at 900□C CuO phase precipitates for x = 0.04 sample indicating that x = 0.03 is the solubility limit for Cu doping in ZnO. The cell parameters of nanoceramics were found to be increased with Cu doping and it varies linearly with increase in Cu concentration. With increase in Cu concentration the crystallite size decreases where as the lattice strain increases. In comparision to uncalcined sample, calcined sample shows increase in crystallite size and decrease in strain.The specific surface area decreases after calcination. The average particle size measured from FESEM is larger than the crystallite size obtained from XRD result. FESEM micrographs demonstrate particle growth with calcination. With increase in duration of milling, the energy band gap decreases. Cu doping results in the red shift of energy band gap of ZnO which shows the Cu doped ZnO samples are suitable for optoelectronics device applications.

# Declarations

### Compliance with Ethical Standards:

The authors declare that they have no conflict of interest.

# References

[1] Calzolari A., Nardell MB. Dielectric properties and Raman spectra of ZnO from a first principles finite-differences/finite-fields approach. *Sci. Rep.* 2013, **3**: 2999.

[2] Fabbiyolaa S, JohnKennedya L, Ratnajia T, JudithVijayac J, Aruldossd U, Bououdinae M. Effect of Fe doping on the structural, optical and magnetic properties of ZnO nanostructures synthesized by co-precipitation method. *Ceram. Int.* 2016, **42**:1588–1596.

[3] Karunakaran C, Vinayagamoorthy P, Jayabharathi J. Optical, electrical, and photocatalytic properties of polyethylene glycol-assisted sol–gel synthesized $BaTiO_3$@ZnO core–shell nanoparticles. *Powder Technol*. 2014, **254**: 480–487.

[4] Ashokkumar M, Muthukumaran S. Tuning of energy gap, microstructure, optical and structural properties of Cr doped $Zn_{0.96}Cu_{0.04}O$ nanoparticles. *Powder Technol.* 2014, **258**: 157–164.

[5] Balamurugan S, Melba K. $Zn_{1-x}Cu_xO$ ($0.02 \leq x \leq 0.1$) Nanomaterials Prepared by Ball Milling, Citrate Sol Gel, and Molten Salt Flux Methods. *J. Nanosci*. Nanotechnol. 2015, **15**:4632-4640.

[6] Ahmad I. Inexpensive and quick phot ocatalytic activity of rare earth (Er, Yb) co-doped ZnO nanoparticles for degradation of methyl orange dye. *Sep. Purif. Technol.* 2019, **227**: 115726.

[7] Singh J, Sharma S., Soni S., Singh RC. Influence of different milling media on structural, morphological and optical properties of the ZnO nanoparticles synthesized by ball milling process. *J. Mater. Synth. Process*. 2019, **98**: 29-38.

[8] Belkhaoui C., Mzabi N., Smaoui H. Investigations on structural, optical and dielectric properties of Mn doped ZnO nanoparticles synthesized by co-precipitation method. *Mater. Res. Bull.* 2019, **111**: 70-79.

[9] Delice S., Isik M., Gasanly NM. Traps distribution in sol-gel synthesized ZnO nanoparticles. *Mater. Lett.* 2019, **245**:103-105.

[10] Agarwal P S. Rai, Gatell EN, Llobet E, Güell F, Kumar M, Awasthi K. Gas sensing properties of ZnO nanostructures (flowers/rods) synthesized by hydrothermal method. *Sens. Actuators, B* 2019, **292**: 24-31.

[11] Han Q., Setchi R., Sam LE. Synthesis and characterisation of advanced ball-milled Al-$Al_2O_3$ nanocomposites for selective laser melting. *Powder Technol.* 2016, **297**:183-192.

[12] Das BK, Das T, Parashar S.K.S. Kumar R., Choudhary HK , Khopkar VB, Anupam AV, Sahoo B. Investigation of structural, morphological and NTCR behaviour of Cu-doped ZnO nanoceramics synthesized by high energy ball milling. *Mater. Chem. Phys.* 2019, **221**: 419-429.

[13] Ramakanth KH. Basics of X-ray Diffraction and its Application. I.K. *International Publishing House Pvt. Ltd.*, New Delhi, 2007. ISBN 13 9788189866075.

[14] Ungar T. Characterization of nanocrystalline materials by X-ray line profile analysis, J. *Mater. Sci.* 2007, **42**:1584.

[15] Suryanarayana C. Mechanical Alloying and Milling. *Marcel Dekker*, New York, 2004.

[16] Cullity BD, Stock SR. Elements of X-ray diffraction, 3rd ed. *Prentice Hall Publication*, India, 2001.

[17] Marotti RE, Guerra DN, Bello C, Machado G., Dalchiele EA. Bandgap energy tuning of electrochemically grown ZnO thin films by thickness and electrodeposition potential. *Sol. Energy Mater. Sol. Cells*. 2004, **82**: 85-103.

[18] Agarwal DC, Chauhan RS, Kumar A, Kabiraj D, Singh F, Khan SA. Synthesis and characterization of ZnO thin film grown by electron beam evaporation. *J. Appl. Phys* 2006, **99**: 123105.

[19] Mishra YK, Chakravadhanula VSK., Hrkac V, Jebril S,. Agarwal DC, Mohapatra S. Crystal growth behavior in Au-ZnO nanocomposite under different annealing environments and photo switchability. *J.Appl. Phys.* 2012, **112**: 064308.

[20] Saw KG, Aznan NM, Yam FK, Ng SS, Pung SY. New Insights on the Burstein-Moss Shift and Band Gap Narrowing in Indium-Doped Zinc Oxide Thin Films. *Plos One* 2015,**10**: 0141180.

[21] Zhu M, Zhang Z, Zhong M, Tariq M, Li Y., Li W. et al. Oxygen vacancy induced ferromagnetism in Cu-doped ZnO. *Ceram. Int*. 2017, **43**: 3166–3170.

[22] Salem M, Massoudi I, Akir S, Litaiem Y, Gaidi M, Khirouni K. Photoelectro chemical and opto-electronic properties tuning of ZnO films: Effect of Cu doping content J. *Alloys Compd.* 2017,**722**: 313–320.

[23] S.S., L. K.C., T. A. Experimental and theoretical investigations of photocatalytic activity of Cu doped ZnO nanoparticles. *Opt. - Int. J. Light Electron Opt.* 2017, **139**: 299–308.

[24] Joshi K, Rawat M, Gautam SK, Singh RG, Ramola RC, Singh F. Band gap widening and narrowing in Cu-doped ZnO thin films. *J. Alloys Compd.* 2016, **680:**252–258.

[25] Wang RC, Lin HY. Cu doped ZnO nanoparticle sheets. *Mater. Chem. Phys.* 2011,**125**: 263–266.

[26] Das BK, Das T, Parashar K, Thirumurugan A, Parashar SKS. Structural, bandgap tuning and electrical properties of Cu doped ZnO nanoparticles synthesized by mechanical alloying. *J. Mater. Sci. Mater. Electron.*, 2017, **28**: 15127–15134.

[27] Prasad N, Karthikeyan B. Cu-doping and annealing effect on the optical properties and enhanced photocatalytic activity of ZnO nanoparticles. *Vacuum.* 2017, **146**: 501–508.

[28] Mhamdi A, Mimouni R, Amlouk A, Amlouk M, Belgacem S. Study of copper doping effects on structural, optical and electrical properties of sprayed ZnO thin films. *J.Alloys Compd.* 2014, **610** : 250–257.

[29] Chen J, Luo L, Lin JS, Zan X, Zhu X, Luo G, Wu Y. Influence of ball milling processing on the microstructure and characteristic of W–Nb alloy. *J. Alloys Compd.*, 2017, **694**: 905–913.

[30] Peleš A, Pavlović VP, Filipović S, Obradović N et al. Structural investigation of mechanically activated ZnO powde. *J. Alloys Compd*. 2015, **648**:971–979.

[31] Liu Y, Yang J, Guan Q et al. Effect of annealing temperature on structure, magnetic properties and optical characteristics in $Zn_{0.97}Cr_{0.03}O$ nanoparticles. *Appl. Surf. Sci*. 2010, **256**:3559–3562.

[32] Das T, Das BK, Parashar K, Kumar R, Choudhary HK, Anupama A. V., Sahoo B, Sahoo PK, Parashar SKS. Effect of Sr-doping on sinterability, morphology, structure, photocatalytic activity and AC conductivity of ZnO ceramics. *J. Mater. Sci. Mater. Electron.* 2017, **28**:13587–13595.

[33] Manikandan A, Judith Vijaya J,. John Kennedy L, Bououdina M. Structural, optical and magnetic properties of $Zn_{1-x}Cu_xFe_2O_4$ nanoparticles prepared by microwave combustion method. *J. Mol. Struct.* 2013,**1035**:332–340.

[34] Das T, Das BK, Parashar SKS, Parashar K. Impact of divalent dopant $Ca^{2+}$ on the electrical properties of ZnO by impedance spectroscopy. *Bull. Mater. Sci.* 2017,**40**: 247–251.

[35] Sung NE, Kang SW, Shin HJ, Lee HK, Lee JJ. Cu doping effects on the electronic and optical properties of Cu-doped ZnO thin films fabricated by radio frequency sputtering. *Thin Solid Films*. 2013, **547**:285–288.

[36] Ghosh A, Kumari N, Tewari S, Bhattacharjee. A Structural, electrical and optical studies on ruthenium doped ZnO pellets for device applications. *Mater. Sci. Eng. B.* 2015,**196**:7–14.

[37] Suwanboon S, Amornpitoksuk P. Preparation of Mg-doped ZnO nanoparticles by mechanical milling and their optical properties. *Procedia Eng.* 2012, **32**: 821–826.

[38] John R, Rajakumari R. Synthesis and Characterization of Rare Earth Ion Doped Nano ZnO. *Nano-Micro Lett.* 2012, **4**:65–72.

[39] Ozgür U, Alivov YI, Liu C et al. A comprehensive review of ZnO materials and devices. *J. Appl. Phys.* 2005, **98**:1–103.

[40] Das T, Das BK, Parashar K, Parashar SKS. Temperature and Frequency Dependence Electrical Properties of $Zn_{1-x}Ca_xO$ Nanoceramic. *Acta Phys. Pol. A*. 2016, **130**: 1358–1362.

[41] Senol SD, Ozturk O, Terzioğlu C. Effect of boron doping on the structural, optical and electrical properties of ZnO nanoparticles produced by the hydrothermal method. *Ceram.Int.* 2015,**41**:11194–11201.

[42] Tan ST, Chen BJ, Sun XW, Fan WJ, Kwok HS, Zhang XH, Chua SJ. Blueshift of optical band gap in ZnO thin films grown by metal-organic chemical-vapor deposition. *J. Appl. Phys.* 2005, **98**:013505.

[43] Kumaresan N, Ramamurthi K, Ramesh Babu R, Sethuraman K, Moorthy Babu S. Hydrothermally grown ZnO nanoparticles for effective photocatalytic activity. *Appl.Surf. Sci.* 2017, **418**:138–146.

[44] Azzez SA, Hassan Z, Hassan JJ, Mukhlif MS, Mahdi MS. Bououdina M. Effect of temperature on hydrothermally grown high-quality single-crystals Mg-doped ZnO nanorods for light-emitting diode application. *J. Lumin.* 2017, **192**:634–643.

[45] Bousslama W, Elhouichet H, Férid M. Enhanced photocatalytic activity of Fe doped ZnO nanocrystals under sunlight irradiation. *Opt. - Int. J. Light Electron Opt.* 2017, **134**:88–98.

[46] Byzynski G, Melo C, Volanti DP, Ferrer MM, Gouveia AF, Ribeiro C, Andrés J. E. Longo, The interplay between morphology and photocatalytic activity in ZnO and N-doped ZnO crystals. *Mater. Des.* 2017, **120**:363–375.

[47] Das S, Roychowdhury A, Das D, Sutradhar S. Effect of Gd doping concentr ation and sintering temperature on structural, optical, dielectric and magnetic properties of hydrothermally synthesized ZnO nanostructure. *J. Alloys Compd*. 2017, **708**:231–246.

[48] Shinde KP, Pawar RC, Sinha BB, Kim HS, Oh SS, Chung KC. Optical and magnetic properties of Ni doped ZnO planetary ball milled nanopowder synthesized by co-precipitation. *Ceram. Int.* 2014, **40**:16799–16804.

[49] Rajender G, Giri PK. Strain induced phase formation, microstructural evolution and bandgap narrowing in strained $TiO_2$ nanocrystals grown by ball milling. *J.Alloys Compd.* 2016, **676**:591–600.

[50] Choi YI, Jung HJ, Shin WG, Sohn Y. Band gap-engineered ZnO and Ag/ZnO by ball-milling method and their photocatalytic and Fenton-like photocatalytic activities. *Appl. Surf. Sci*. 2015, **356**:615–625.

[51] Yu W, Zhang J, Peng T. New insight into the enhanced photocatalytic activity of N, C and S-doped ZnO photocatalysts. *Appl. Catal. B-Environmental.* 2016, **181**:220–227.

[52] Matsunami N, Itoh M, Kato M, Okayasu S, Sataka M, Kakiuchida H. Applied Surface Science Growth of Mn-doped ZnO thin films by rf-sputter deposition and lattice relaxation by energetic ion impact. *Appl. Surf. Sci.* 2015, **350**:31–37.

[53] Juma A, Oja Acik I, Oluwabi AT, Mere A, Mikli V, Danilson M, Krunks M. Zirconium doped $TiO_2$ thin films deposited by chemical spray pyrolysis. *Appl.Surf.Sci.* 2016, **387**:539–545.

[54] Ghosh A, N. Kumari, S. Tewari, A. Bhattacharjee. Structural, electrical and optical studies on ruthenium doped ZnO pellets for device applications. *Mater. Sci. Eng. B*. 2015,**196**:7–14.

[55] Diouri J, Lascaray JP, El Amrani M. Effect of the Magnetic Order on the Optical-Absorption Edge in $Cd_{1-x}Mn_xTe$. *Phys. Rev. B.* 1985, **31**:7995–7999.

[56] Li XY, Li HJ, Yuan M, Wang ZJ, Zhou ZY, Xu RB. Influence of oxygen partial pressure on electrical and optical properties of $Zn_{(0.93)}Mn_{(0.07)}O$ thin films. *J. Alloys Compd.* 2011, **509**:3025–3031.

[57] Elilarassi R, Chandrasekaran G. Structural, optical and magnetic characterization of Cu-doped ZnO nanoparticles synthesized using solid state reaction method. *J. Mater. Sci. Mater. Electron.* 2010, **21**:1168–1173.

[58] Ferhat M, Zaoui A, Ahuja R. Magnetism and band gap narrowing in Cu-doped ZnO. *Appl. Phys. Lett.* 2009, **94**:1–4.

[59] Bylsma RB, Becker MW, Kossut J, Debska U, Yoder-Short D. Dependence of energy gap on x and T in $Zn_{1-x}Mn_xSe$: The role of exchange interaction. *Phys. Rev.B.* 1986, **33**:8207–8215.

# Figures

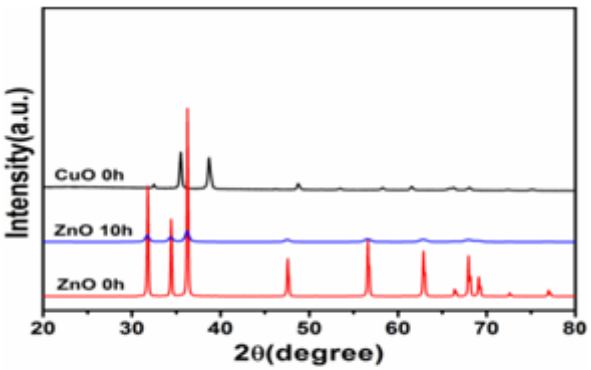


**Figure 1**

**Figure 1**

XRD pattern of pure ZnO, pure CuO and 10h ball milled ZnO samples.

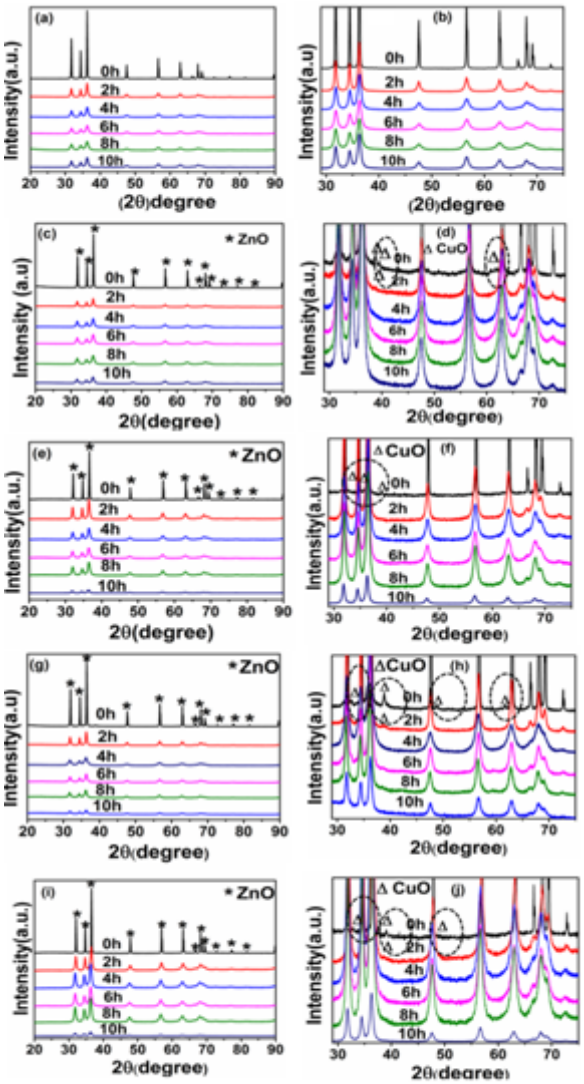


**Figure 2**

## Figure 2

XRD patterns of Zn1-xCuxO (x = 0 - 0.04) nanoceramics with different milling time:(a) x = 0, (b) enlarged view of (a), (c) x = 0.01, (d) enlarged view of (c), (e) x = 0.02, (f) enlarged view of (e), (g) x = 0.03, (h) enlarged view of (g), (i) x = 0.04 and (j) enlarged view of (i).

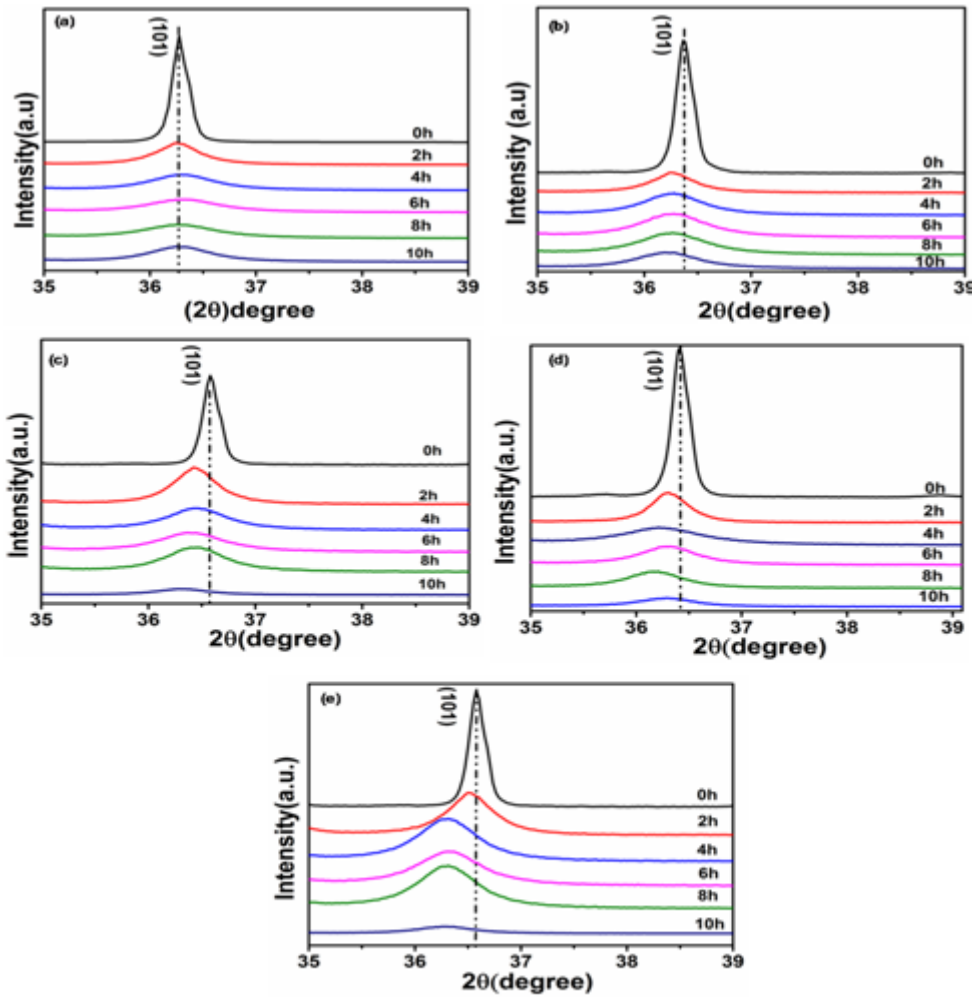


**Figure 3**

## Figure 3

XRD peak shifting of most intense peak of Zn1-xCuxO (a) x = 0, (b) x = 0.01, (c) x = 0.02, (d) x = 0.03 and (e) x = 0.04 nanoceramics with different milling time.

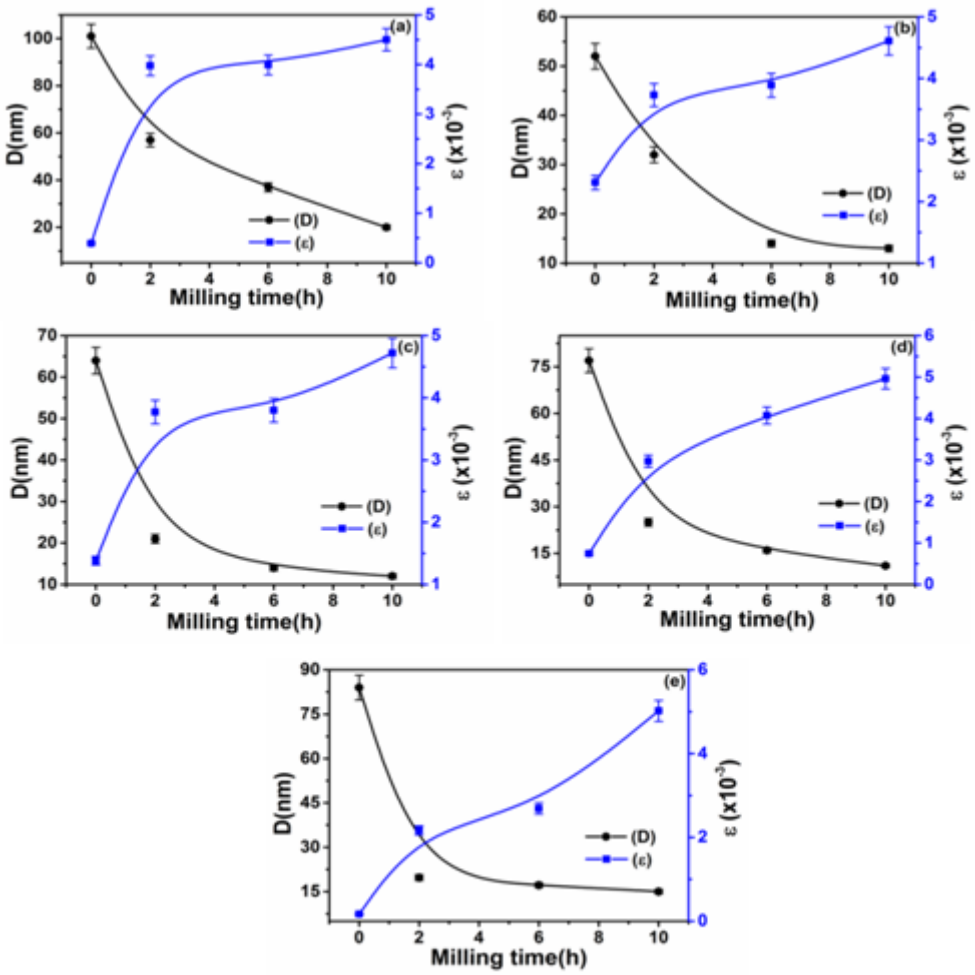


**Figure 4**

## Figure 4

The crystallite size and strain variation with different milling time of Zn1-xCuxO nanoceramics: (a) x = 0, (b) x = 0.01, (c) x = 0.02, (d) x = 0.03 and (e) x = 0.04

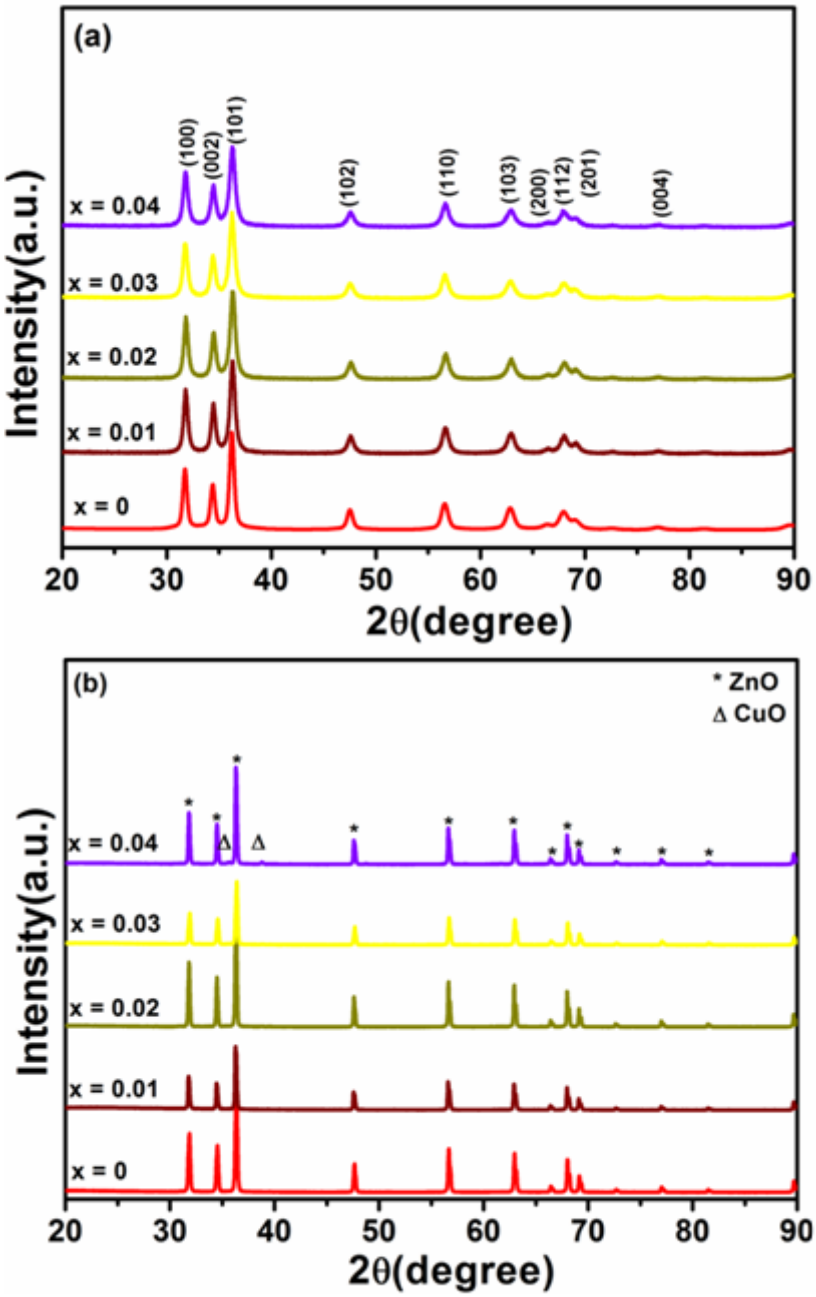


**Figure 5**

## Figure 5

X-ray diffraction of Zn1-xCuxO nanoceramics (a) after 10h ball milling and (b) after 10h ball milling and calcination at 900 ºC for 2h.

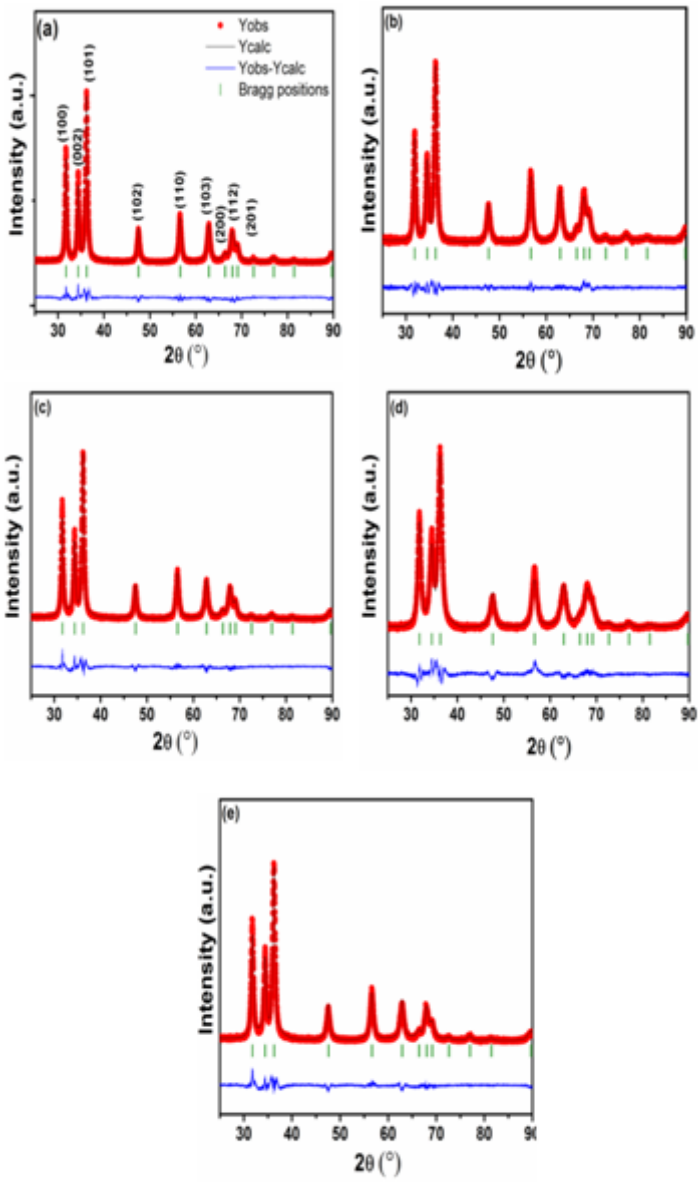


**Figure 6**

## Figure 6

XRD patterns of 10h milled Cu doped ZnO (Zn1-xCuxO) nanoceramics obtained by Rietveld refinement: (a) x = 0, (b) x = 0.01 (c) x = 0.02 (c) x = 0.03, (d) x = 0.03 and (e) x = 0.04.

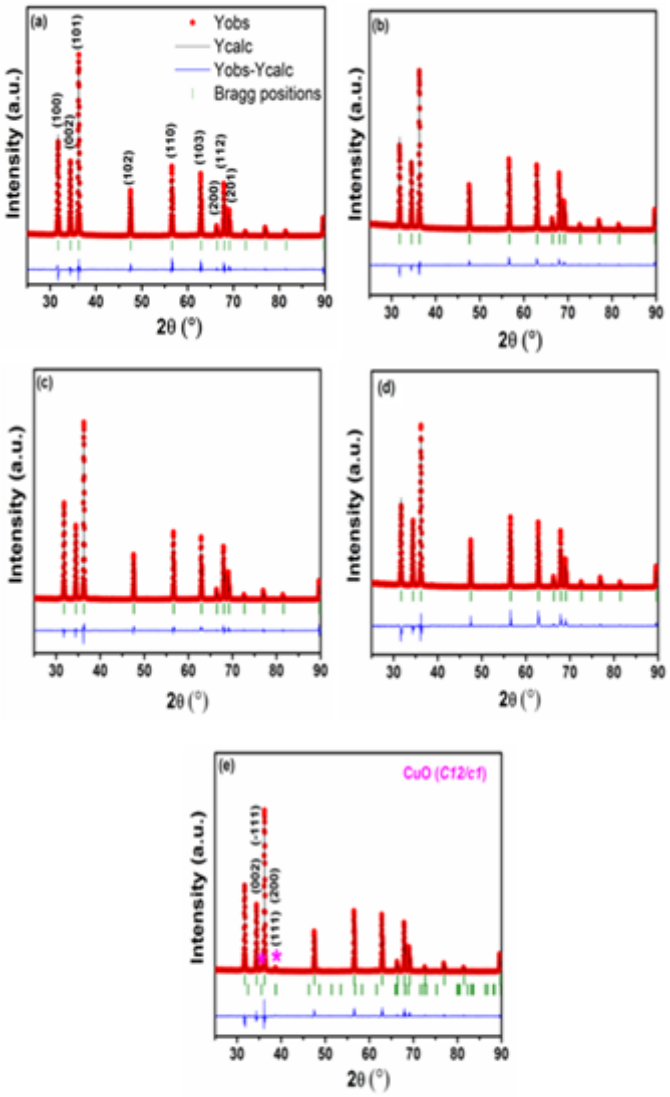


**Figure 7**

## Figure 7

Rietveld refined XRD patterns of 10h milled 900ºC calcined Zn1-xCuxO nanoceramics: (a) x = 0, (b) x = 0.01 (c) x = 0.02 (c) x = 0.03, (d) x = 0.03 and (e) x = 0.04.

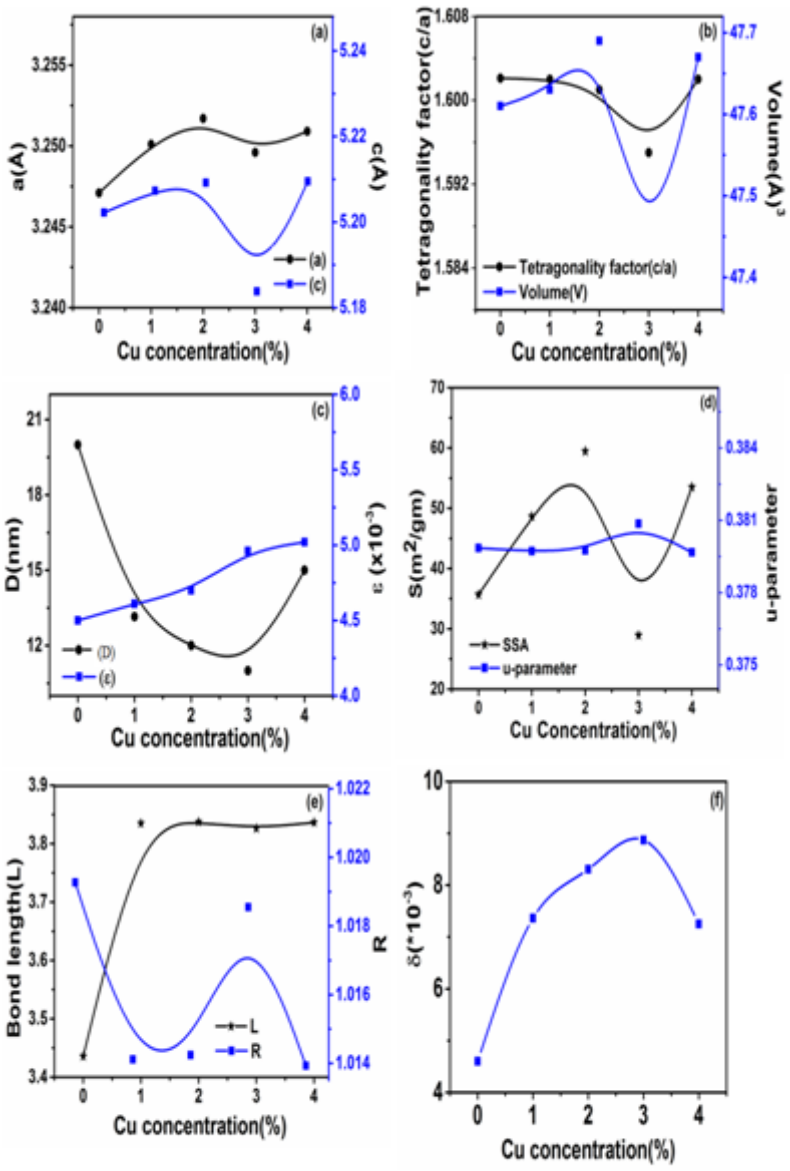


**Figure 8**

## Figure 8

Variation of structural parameters with Cu concentration of 10h ball milled Zn1-xCuxO (x = 0, 0.01, 0.02, 0.03 and 0.04) nanoceramics: (a) lattice constant ‘a’ and ‘c’, (b) tetragonality factor (c/a) and volume (V), (c) crystallite size (D) and strain (ε), (d) specific surface area (S) and u-parameter, (e) bond length (L) and crystal lattice distortion degree (R) and (f) dislocation density (δ).

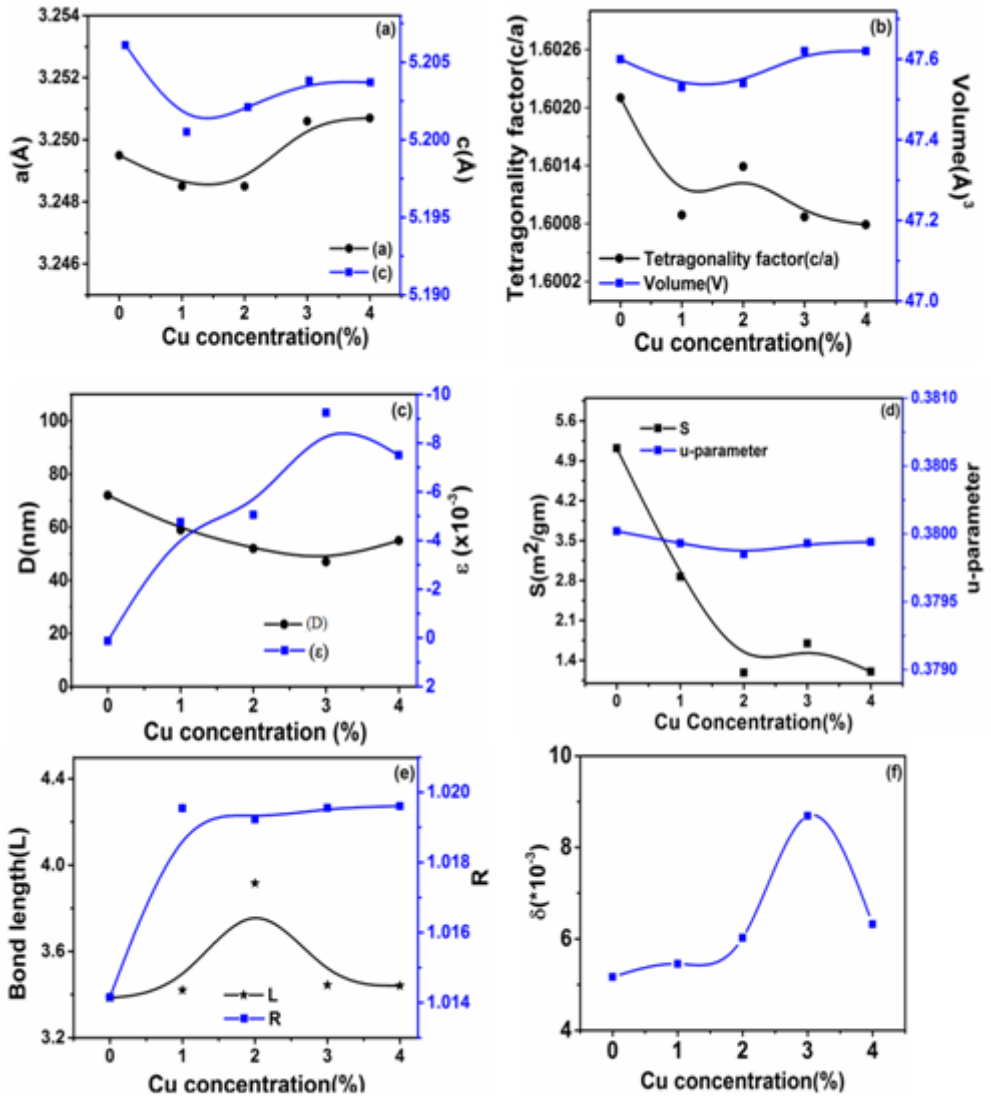


**Figure 9**

## Figure 9

Variation of structural parameters with Cu concentration of 10h ball milled calcined Zn1-xCuxO nanoceramics: (a) lattice constant ‘a’ and ‘c’, (b) tetragonality factor (c/a) and volume (V), (c) crystallite size (D) and strain (ε), (d) specific surface area (S) and u-parameter, (e) bond length (L) and crystal lattice distortion degree (R) and (f) dislocation density (δ).

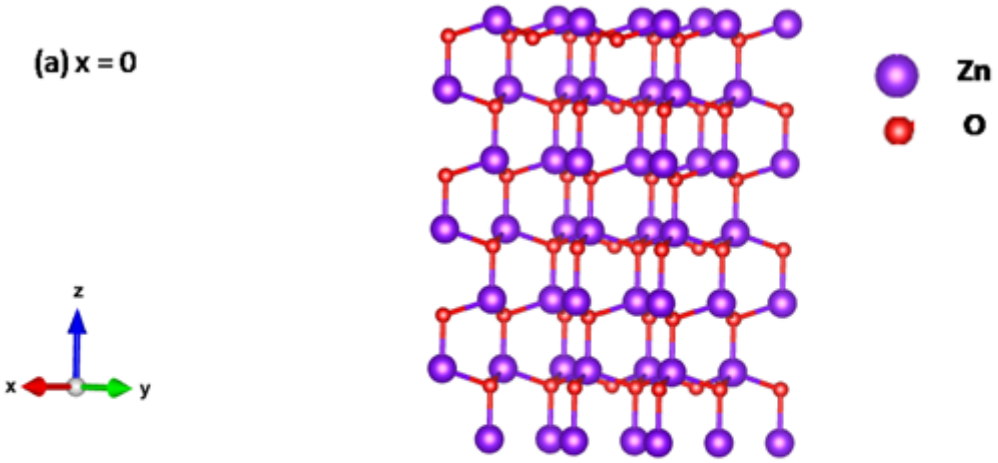


**Figure 10**

## Figure 10

Wurtzite supercell of 10h milled ZnO powder.

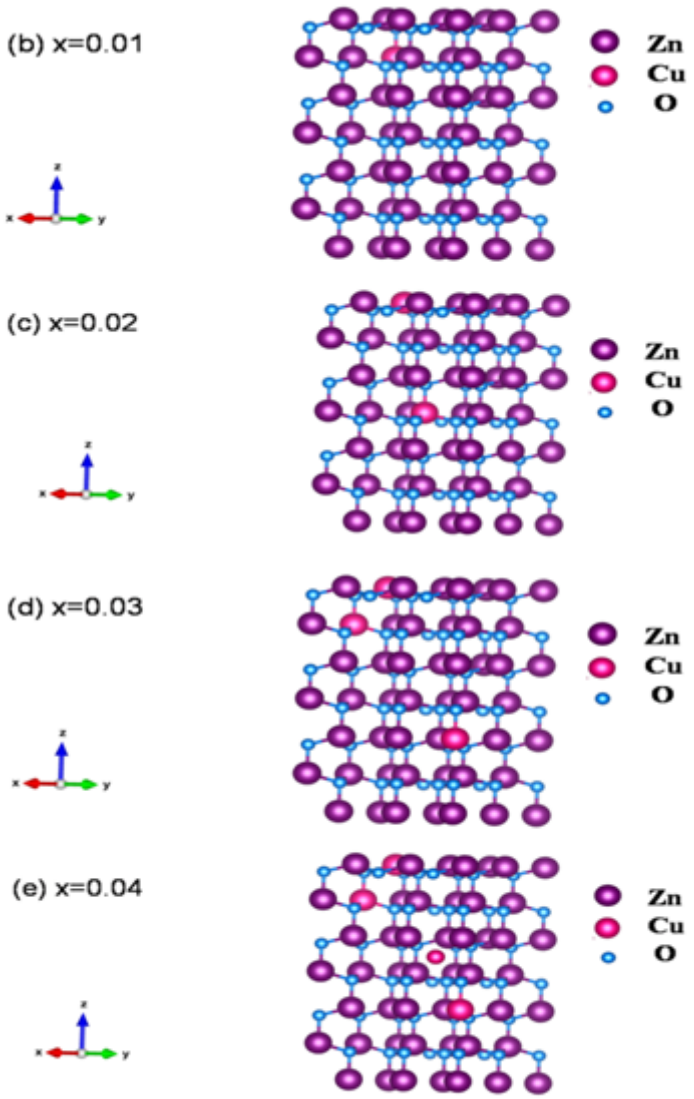


Figure 11

## Figure 11

Wurtzite supercells of 10h milled powder of Zn1-xCuxO: (b) x = 0.01, (c) x = 0.02, (d) x = 0.03 and (e) x = 0.04.

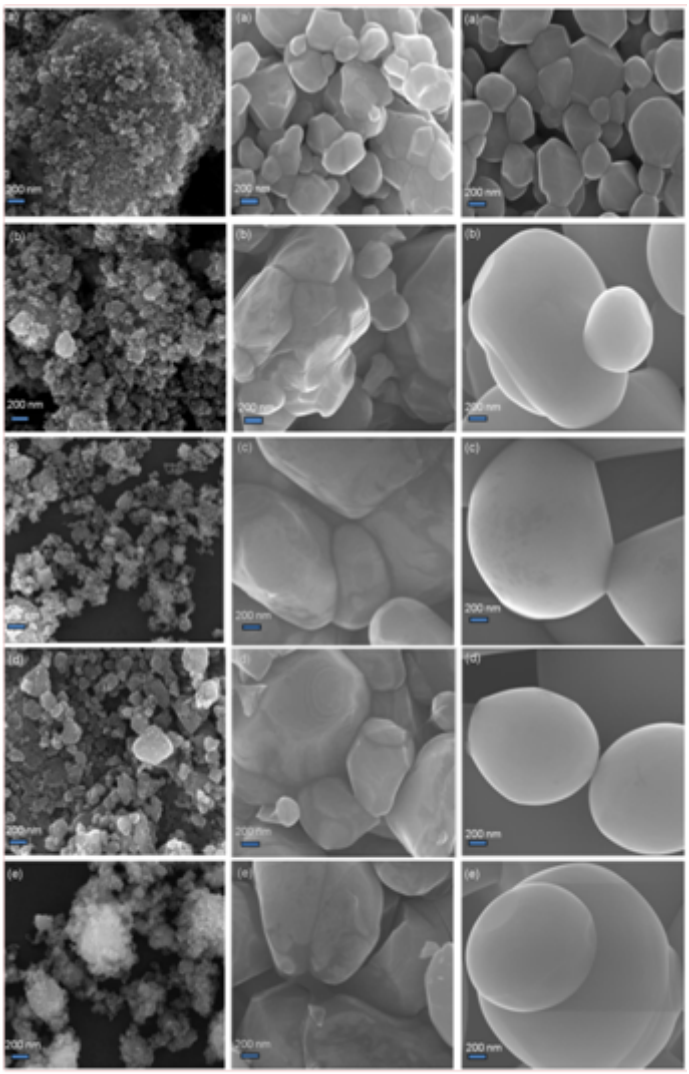

Figure 12

## Figure 12

FESEM micrograph of 10h milled Zn1−xCuxO nanoceramics with different Cu concentration, (a) x = 0, (b) x = 0.01, (c) x = 0.02, (d) x = 0.03, (e) x = 0.04): (i) uncalcined sample,(ii) pellet of calcined (900 ºC) sample and (iii) calcined and sintered (900 ºC) pellet.

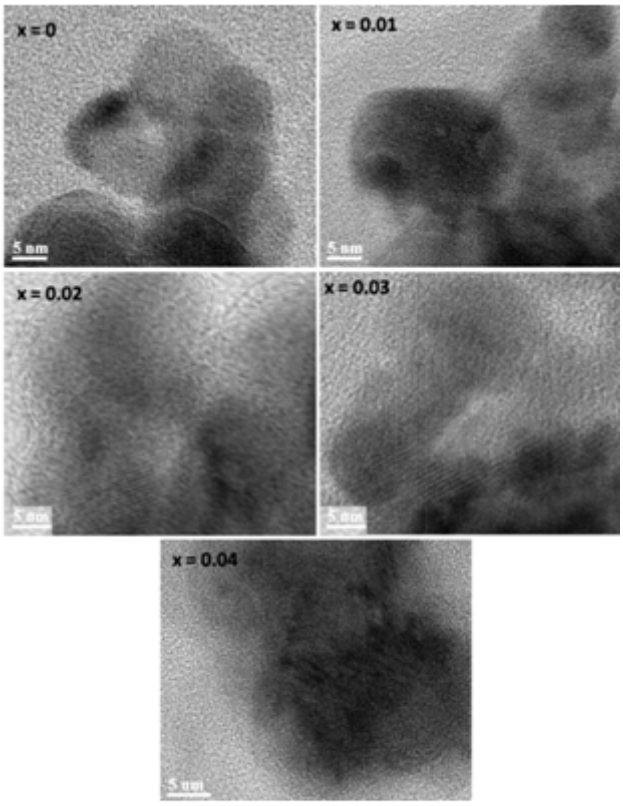


**Figure 13**

## Figure 13

TEM micrographs of 10h milled Zn1-xCuxO (x = 0, 0.01, 0.02, 0.03, 0.04) nanoceramics.

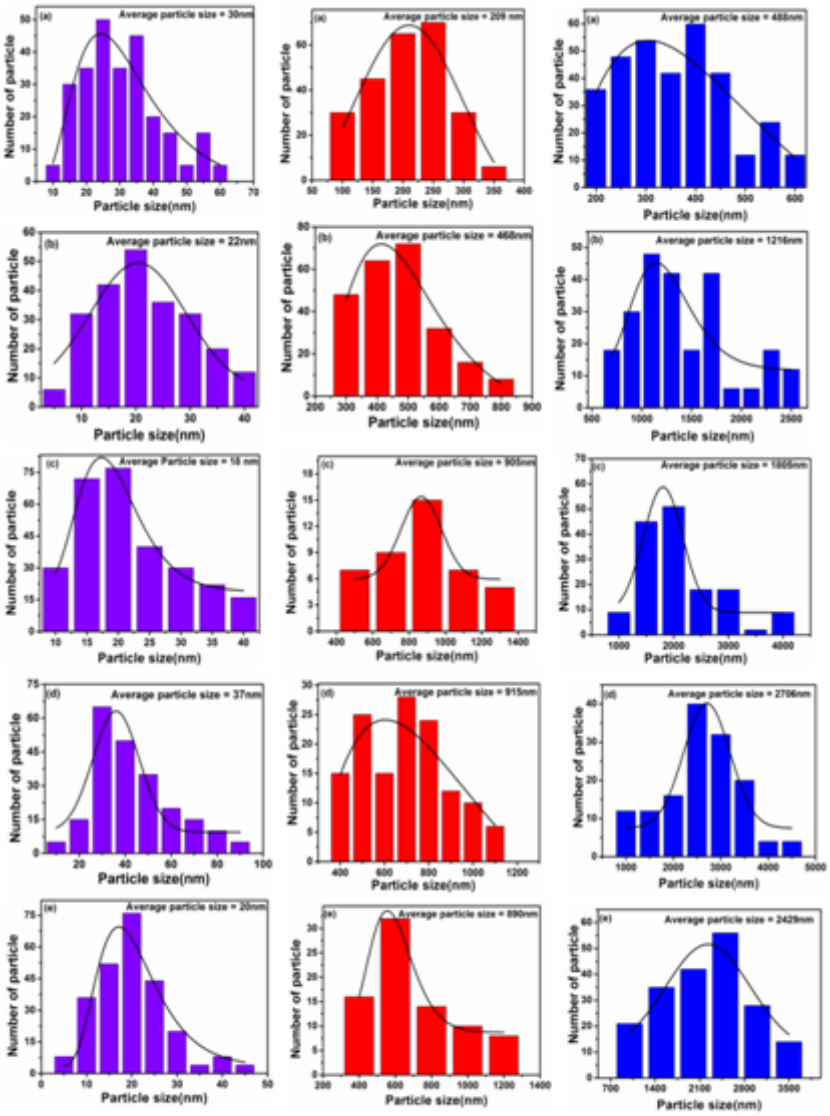


**Figure 14**

## Figure 14

Particle size distribution of 10h milled Zn1−xCuxO nanoceramics with different Cu concentration, (a) x = 0, (b) x = 0.01, (c) x = 0.02, (d) x = 0.03, (e) x = 0.04): (i) uncalcined powder, (ii) pellet of calcined (900 ºC) powder and (iii) calcined and sintered (900 ºC) pellet.

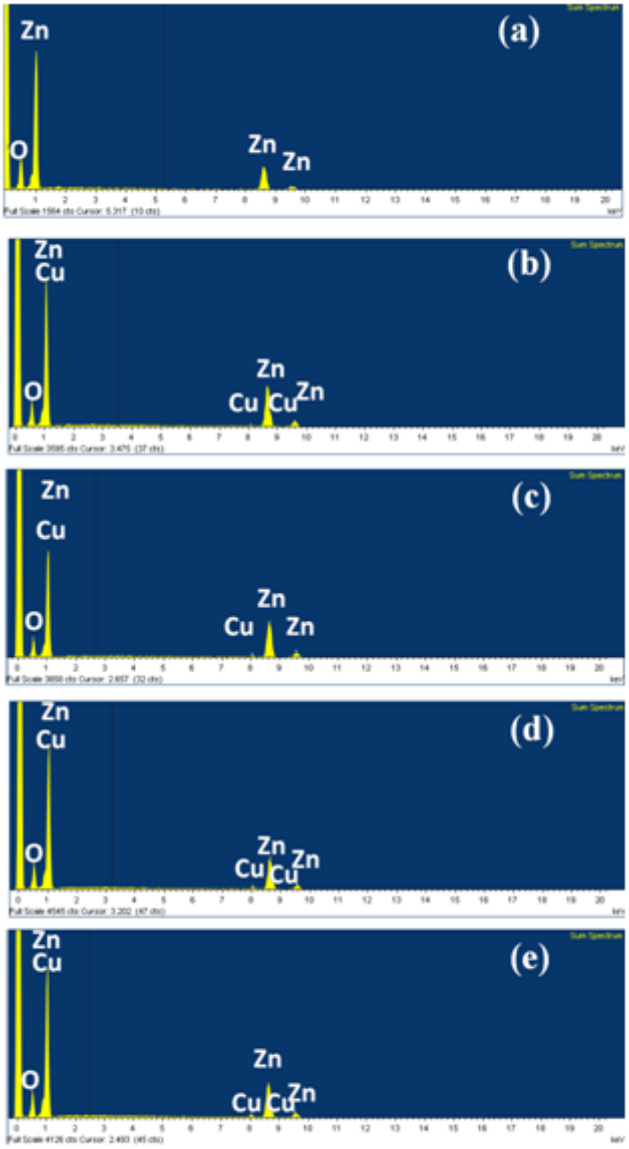


**Figure 15**

## Figure 15

EDX pattern of 10h milled Zn1-xCuxO nanoceramics: (a) x = 0 (b) x = 0. 01 (c) x = 0.02 (d) x = 0.03 and (e) x = 0.04.

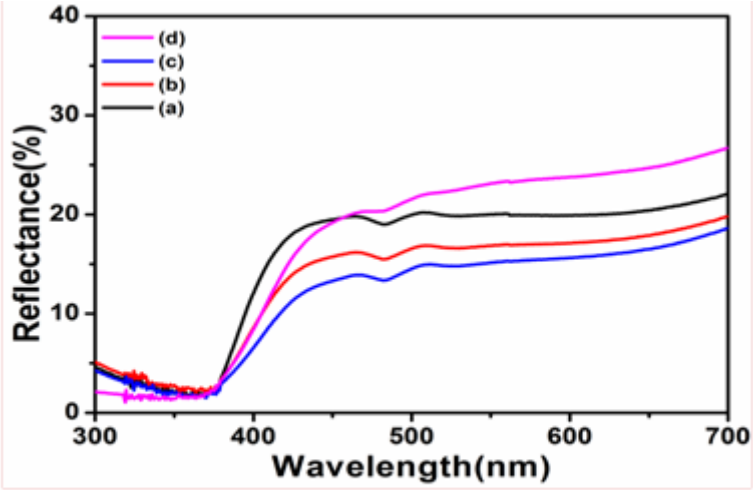


Figure 16

Figure 16

Reflectance spectra of 2% Cu doped ZnO powder sample at different duration of milling (a) 2h, (b) 4h, (c) 8h and (d) 10h.

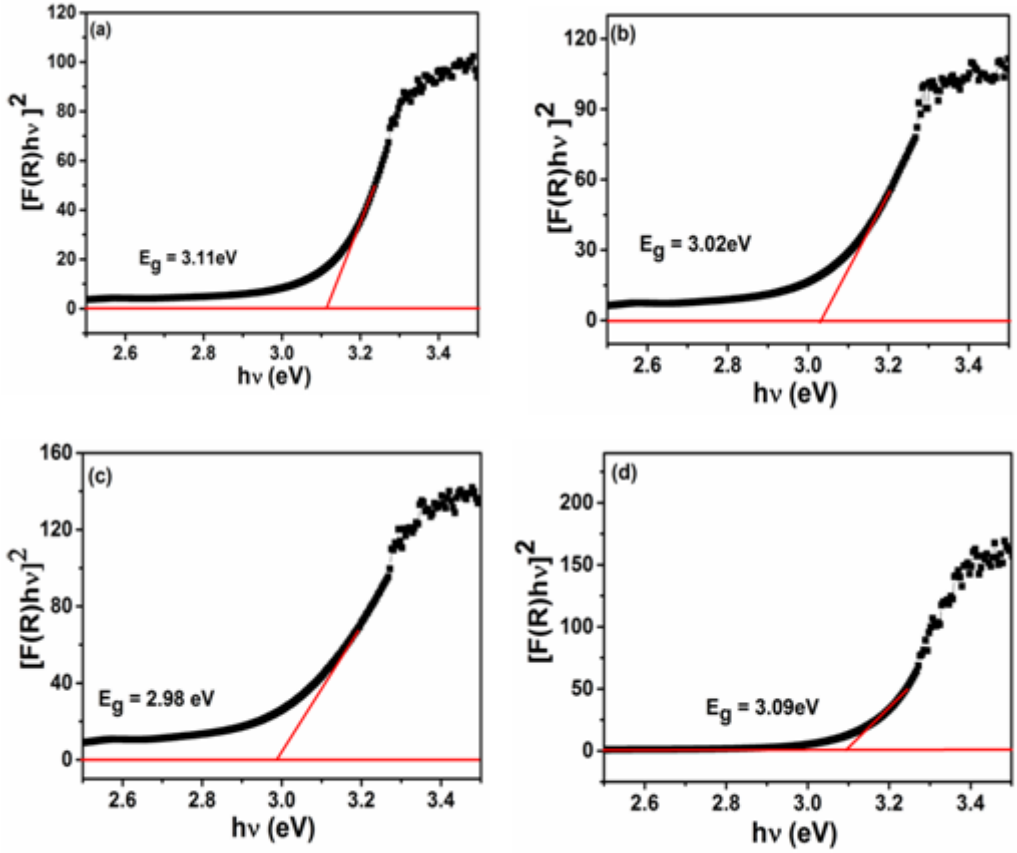


Figure 17

Figure 17

The optical energy band gap of 2% powder sample of Cu doped ZnO at different duration of milling (a) 2h, (b) 4h, (c) 8h and (d) 10h.

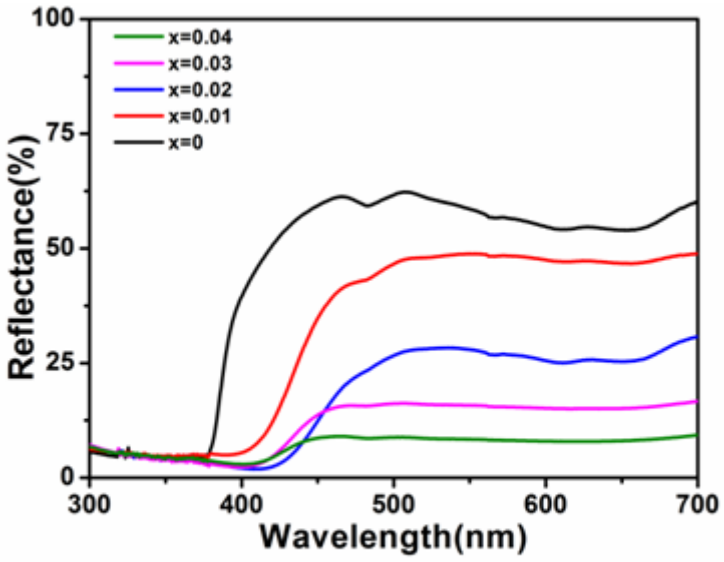


**Figure 18**

**Figure 18**

Reflectance spectra of 10h milled powder after calcination at 900ºC of Zn1-xCuxO (x = 0, 0.01, 0.02, 0.03 and 0.04) nanoceramics.

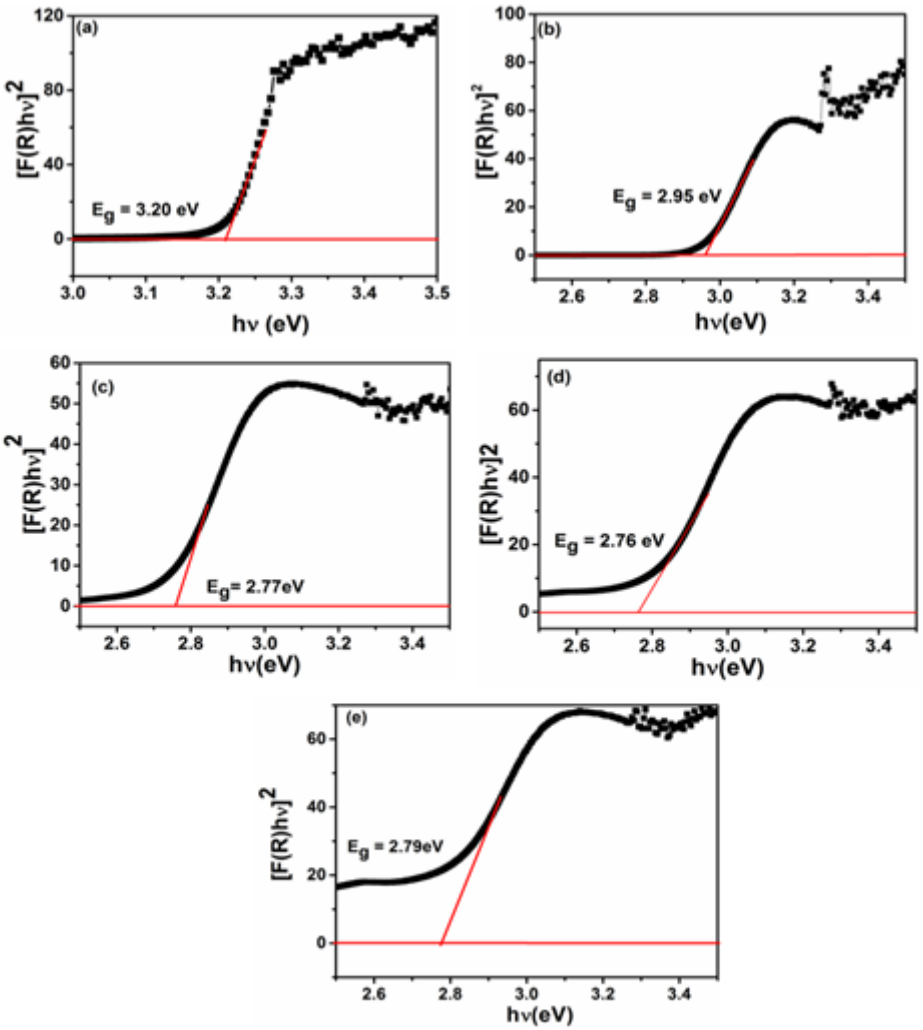


**Figure 19**

**Figure 19**

The optical energy band gap of 10h milled calcined Zn1-xCuxO nanoceramics: (a) x = 0, (b) x = 0.01, (c) x = 0.02, (d) x = 0.03 and (e) x = 0.04.

# Supplementary Files

This is a list of supplementary files associated with this preprint. Click to download.

- GraphicalAbstract.cu.tif